

# Low-Profile Circularly Polarized Cavity-Backed Antennas Using SIW Techniques

Qi Wu, *Student Member, IEEE*, Haiming Wang, *Member, IEEE*, Chen Yu, *Member, IEEE*, and Wei Hong, *Fellow, IEEE*

**Abstract**—Two single fed low-profile cavity-backed slot antennas and an antenna array for circular polarization (CP) applications are introduced. By employing the substrate-integrated waveguide (SIW) and half-mode SIW (HMSIW) techniques in antenna designs, low-profile cavity-backed structures are realized using the low-cost standard printed circuit board process. First, a novel spoon-shaped slot antenna is proposed to realize CP radiation based on the SIW cavity. Then, to minimize the antenna size and achieve the impedance bandwidth enhancement, the HMSIW cavity is introduced to realize a cavity-backed semicircle slot antenna (SSA). The equivalence between the edge of the HMSIW cavity and the longitude slot curved on the surface of the SIW cavity is proposed to guide the design process of the SSA. In addition, two hybrid modes are used to improve the impedance bandwidth of the SSA. Furthermore, a sequential rotation antenna array is introduced to validate the feasibility of the SSA for antenna array application. Finally, the proposed antennas and the antenna array are designed and fabricated at 28 GHz. The measured and simulated results agree very well.

**Index Terms**—Array antenna, cavity-backed antennas, circular polarization (CP), half-mode substrate-integrated waveguide (HMSIW), SIW.

## I. INTRODUCTION

AS THE demand for capacity in mobile communications increases dramatically, mobile carriers are facing a big challenge of the significant increase of mobile traffics. Recently, super high frequency (3~30 GHz) and extremely high frequency (30~300 GHz) communications, which offer possible multiple gigabit-per-second data transmission, have attracted great attention for the future wireless communications [1]–[3]. Several antenna structures have been proposed for different wireless communication scenes, such as

Manuscript received December 23, 2015; revised March 19, 2016; accepted April 23, 2016. Date of publication April 29, 2016; date of current version July 5, 2016. This work was supported in part by the Strategic Emerging Industry Development Funds of Shenzhen of China under Grant ZDSYS20140509094955257, in part by the National Key Basic Research Program of China (973 Program) under Grant 2013CB329002, in part by the Natural Science Foundation of Jiangsu Province of China under Grant BE2015156 and Grant BK20130631, in part by the National 863 Program of China under Grant 2015AA01A703, and in part by the National Natural Science Foundation of China under Grant 61132003 and Grant 61132003. (*Corresponding author: Haiming Wang*)

Q. Wu, C. Yu, and W. Hong are with the State Key Laboratory of Millimeter Waves, Southeast University, Nanjing 210096, China (e-mail: qiwu@seu.edu.cn; chenyu@seu.edu.cn; weihong@seu.edu.cn).

H. Wang is with the State Key Laboratory of Millimeter Waves, Southeast University, Nanjing 210096, China, and also with ZTE Wavetone Science and Technology Ltd., Nanjing 211111, China (e-mail: hmwang@seu.edu.cn).

Color versions of one or more of the figures in this paper are available online at <http://ieeexplore.ieee.org>.

Digital Object Identifier 10.1109/TAP.2016.2560940

cellular devices [3], [4] and base stations [5]. Using a compact, low-profile, and circular polarization (CP) antenna with stabilized gain and good return loss character is a possible solution for the future wireless communication applications, due to its convenience to integrate with the compact user equipments and overcome the problem of polarization mismatch.

As a high-gain antenna structure, the cavity-backed antennas have been widely investigated [6]–[8]. Although the conventional cavity-backed antennas have the good radiation performance, they always suffer from bulky structures, expensive manufacturing expenses, and hard to integrate with planar circuits. In order to overcome these drawbacks, the substrate-integrated waveguide (SIW) technique has been applied to the cavity-backed CP antenna designs. Recently, the SIW structure has been widely used in planar passive components and antennas [9]. Many SIW-cavity-backed CP antennas have been investigated [10]–[14]. An X-band ring-slot cavity-backed SIW antenna using a shorting pin to generate CP radiation was designed [10] and fabricated into antenna arrays [11] for satellite communication applications. Crossed slots were used in the SIW cavities to develop dual linearly polarization or CP radiation [12]. With a dual-mode triangular-ring slot, a dual-band CP SIW cavity antenna was achieved [13]. While the previously suggested structures exhibit good electrical performances, only few of them present a broad impedance bandwidth [14].

While the SIW introduces a fresh way to solve the bulky of the cavity-backed antenna design, its size may still be large for some specific applications. The half-mode SIW (HMSIW) structure has been proposed to overcome the size problem [15], which reduces the size of the SIW structure by nearly 50% without weakening its performance. Several antenna designs have been proposed based on the HMSIW structures [16]–[20]. The HMSIW structure has been found its application in the traveling-wave antenna [17] and leaky-wave antenna [18], [19] designs. As for the cavity-backed antennas, two transverse slots were introduced in the HMSIW cavity to produce dual-band operation in on-body scenes [20]. By introducing two orthogonal quarter-wavelength patch modes, a simple single-fed HMSIW cavity-backed CP antenna was proposed in [16]. However, when compared with some of the conventional SIW cavity designs [14], the cavity-backed slot CP antennas based on the HMSIW technique still suffers from low gain and narrow bandwidth [16].

Among various kinds of radiation structures, the ring slot element has been widely investigated. Using the dual-ring

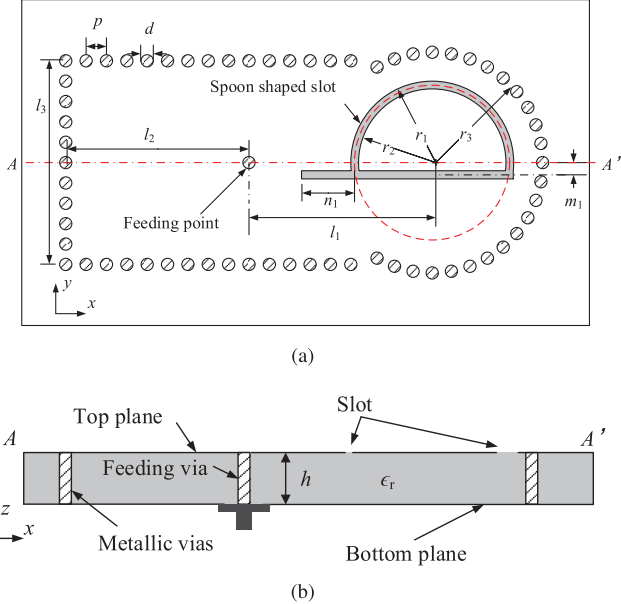


Fig. 1. Configurations of the proposed SIW cavity-based SSSA. (a) Top view. (b) Side view.

structure [21] or the shorted point [7], annular-ring slot antennas could achieve dual-band operation or radiate far field CP wave. Combined slot/strip loop was introduced to achieve broadband CP performance [22]. Multiple feeding lines, such as coplanar waveguide [23], microstrip [24], and SIW [10], were introduced to realize quasi-ring slot structures.

The sequential rotation technique has been usually used to improve both the axial ratio (AR) and the impedance bandwidth. Compared with the linearly polarized element-based sequential rotated array, the CP elements-based array present a broader AR and impedance bandwidth, and a higher peak gain [25], [26]. Sequential rotation arrays with various kinds of CP element structures, including the dielectric resonator antenna [27], microstrip patch antenna [25], and SIW cavity-backed antenna [11] arrays, have been extensively studied.

In this paper, the SIW and HMSIW techniques are utilized to realize the cavity-backed planar slot CP antennas and an antenna array. Section II discusses the design and optimization of the two cavity-backed antenna elements. First, a spoon-shaped slot antenna (SSSA) based on the SIW cavity is proposed to achieve CP radiation. Next, a semicircle slot antenna (SSA) based on the HMSIW cavity is introduced to realize CP radiation with a more compact size. In Section III, the prototypes of the antenna elements and an SSA-based sequential rotation antenna array are fabricated. The measured results are discussed in Section IV. Section V covers the conclusion of the proposed designs.

## II. ANTENNA ELEMENT DESIGN

### A. Spoon-Shaped Slot Antenna

The structure of the SSSA is shown in Fig. 1. The dimensions of the proposed SSSA are shown in Table I. The proposed SSSA is simply composed of an SIW cavity and a spoon-shaped slot curved on the surface of the cavity.

TABLE I  
PARAMETERS OF THE PRESENTED SSSA

Parameter	Value (mm)	Parameter	Value (mm)
$r_1$	2.00	$n_1$	1.20
$r_2$	1.80	$m_1$	0.21
$r_3$	2.75	$l_1$	4.50
$p$	0.50	$l_2$	4.50
$d$	0.30	$l_3$	5.00
$h$	0.51	$\epsilon_r$	2.20

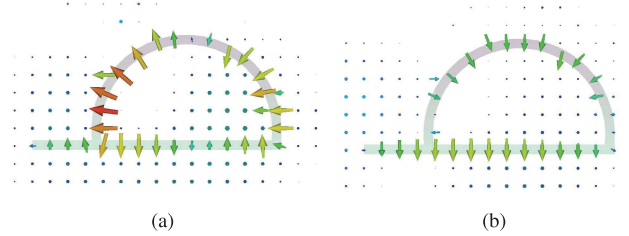


Fig. 2. Simulated  $\vec{E}$  at the slot of SSSA at 28 GHz when (a) phase = 0° and (b) phase = 90°.

The SIW cavity formed by metallic vias acts as a perfect electric wall. The spoon-shaped slot includes a longitudinal line slot and a portion of a circular ring-slot cut by the longitudinal line. As shown in Fig. 1, the offset of the longitudinal line from the central line of the SIW cavity is denoted by  $m_1$ , and the excessive offset of the longitudinal line slot aside from the edge of the ring slot is represented by  $n_1$ .

The fundamental  $\text{TM}_{010}$  mode is selected as the working mode of the circular SIW cavity. The radius of the circular SIW cavity  $r_3$  can be deduced by [28]

$$f_{010} = \frac{c}{2\pi\sqrt{\mu_r\epsilon_r}} \cdot \frac{p_{01}}{R} \quad (1)$$

where  $f_{010}$  is the resonant frequency of the  $\text{TM}_{010}$  mode,  $c$  is the velocity of light in the vacuum,  $p_{01}$  is the 1th root of 0th Bessel function of the first kind,  $R \approx r_3$  is the radius of circular cavity, and  $\mu_r$  and  $\epsilon_r$  are the relative permeability constant and the relative dielectric constant of the substrate of the SIW cavity, respectively.

The annular-ring-like slot exhibits similar working mode with the conventional ring-slot structure. As shown in Fig. 2, the electric field distribution in the spoon-shaped slot is similar to that of the first-operating mode in the annular-ring slot. The center CP operating frequency  $f_{cp}$  can be determined using

$$f_{cp} = \frac{1.4c}{2\pi r_e\sqrt{\epsilon_e}} \quad (2)$$

where  $r_e = (r_1 + r_2)/2$ , and  $\epsilon_e = (\epsilon_r + 1)/2$ . This SSSA dimension formula is a slight modification to the one presented in [24]. The coefficient 1.5 is modified by 1.4 similar to the statement in [29], and the  $\epsilon_e$  approximation is modified on account of the SIW cavity structure, which denotes the effective relative dielectric constant of the slot [13]. Equation (2) provides a reasonable accuracy in the designated frequency of 28 GHz.

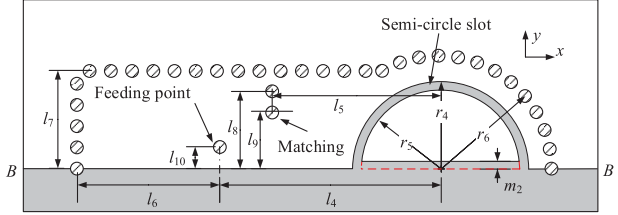


Fig. 3. Top view of the proposed SSA.

TABLE II  
PARAMETERS OF THE PRESENTED SSA

Parameter	Value (mm)	Parameter	Value (mm)
$r_4$	1.99	$l_7$	2.50
$r_5$	1.79	$l_8$	1.30
$r_6$	2.66	$l_9$	0.80
$l_4$	5.02	$l_{10}$	0.60
$l_5$	3.52	$m_2$	0
$l_6$	3.50		

In order to demonstrate the radiation performance of the structure, the electric field  $\vec{E}$  at the slot is investigated. Fig. 2 shows the electric field of the slot within half a period. As shown in Fig. 2(a), when the phase equals  $0^\circ$ , the electric field along the longitudinal slot line slot counteracts with itself and the resonance along the annular slot takes charge, while the resonance of the longitudinal slot line takes charge when the phase turns to  $90^\circ$ , as shown in Fig. 2(b). A counterclockwise-rotated equivalent magnetic current distribution can be seen moving along the slot. In addition, the antenna radiates an right-hand circular polarization (RHCP) wave at the  $+z$ -axis. Similarly, an left-hand circular polarization (LHCP) radiation can be achieved when the spoon-shaped structure is mirrored within the central line of the SIW cavity.

#### B. Semicircle Slot Antenna

While the proposed SSSA exhibits good electrical performances, it still suffers from relatively narrow impedance bandwidth and large size for some applications. To overcome these disadvantages, the HMSIW structure is introduced in the antenna design process. The top view of the proposed SSA is shown in Fig. 3, and the side view of the SSA is similar to that of the SSSA in Fig. 1(b). The antenna element is simply composed of an HMSIW cavity with a matching circuit and a semicircle ring-slot curved at the surface of the cavity. A parameter  $m_2$  acts as a tuner is introduced in the antenna design, which represents the distance between the edge of the quasi-semicircle patch and the edge of the HMSIW. The dimensions of the proposed SSA are shown in Table II.

The topology of the SSA stems from the SSSA. Fig. 4 shows how an SSSA backed by an SIW cavity is transformed into the SSA backed by an HMSIW cavity. Given the symmetry of the electric field distribution in the SIW cavity, the symmetry plane in the cavity behaves as a virtual magnetic wall. Therefore, the SIW cavity can be split along the symmetry plane, leading to a size reduction of

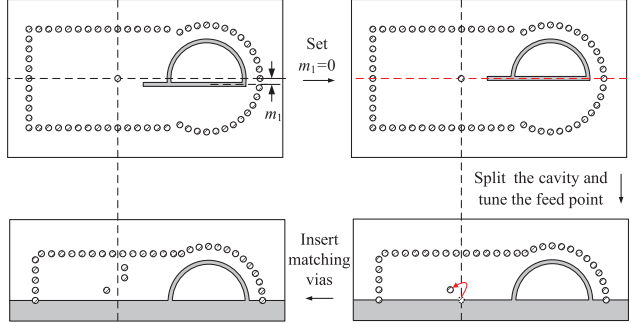
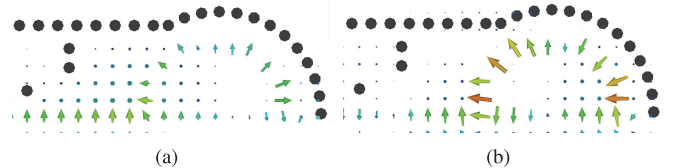


Fig. 4. Transformation from the SSSA to the SSA.

Fig. 5. Simulated  $\vec{E}$  at the slot and edge of the SSA at 28 GHz when (a) phase =  $0^\circ$  and (b) phase =  $90^\circ$ .

almost 50% without significant loss in the feeding structure. Moreover, by setting  $m_1 = 0$ , the longitudinal line slot in SSSA is placed along the symmetry plane of the SIW cavity, and then replaced by the edge of HMSIW in the SSA. This transformation comes from the similar radiation character of these two structures. Moreover, the feed point is slightly tuned to excite the HMSIW cavity, and the matching circuit is inserted to achieve better matching performance.

The initial dimensions of the slot on the SSA can also be determined by (2), where  $r_e = (r_4 + r_5)/2$ . This formula provides a reasonable accuracy in the designated frequency of 28 GHz. As for the half-mode semicircle cavity, it shows similar frequency characteristics of the half TM<sub>010</sub> mode with the original circle cavity used in SSSA TM<sub>010</sub> mode. Thus, the radius of the HMSIW cavity  $r_6$  can also be determined by (1), where  $R \approx r_6$ . Compared with the SSSA, the SSA presents a similar CP radiation performance, but a much broader reflection coefficient bandwidth. The reasons are as follows.

First, similar to the SSSA, the SSA exhibits CP radiation character in the designed frequency. The equivalent magnetic current along the semicircle slot and the cutting edge of the HMSIW can be represented by the electric field above them. Fig. 5 shows the simulated  $\vec{E}$  at the surface of the proposed SSA structure, which indicates that the edge of the HMSIW in the SSA plays the same role as the longitudinal line slot in the SSSA. With the similar electric field with the SSSA, the SSA radiates an RHCP wave at the  $+z$ -axis. An LHCP wave can be achieved when the semicircle slot structure and the HMSIW cavity are mirrored within the edge line of the HMSIW cavity.

Second, different from the structure in the SSSA, the introduction of the HMSIW leads to the loss of the shunt admittance impact brought by the offset of the longitudinal line slot aside from the symmetry plane of the SIW cavity in the SSSA, which is calibrated by  $m_1$ . Fig. 6 shows the

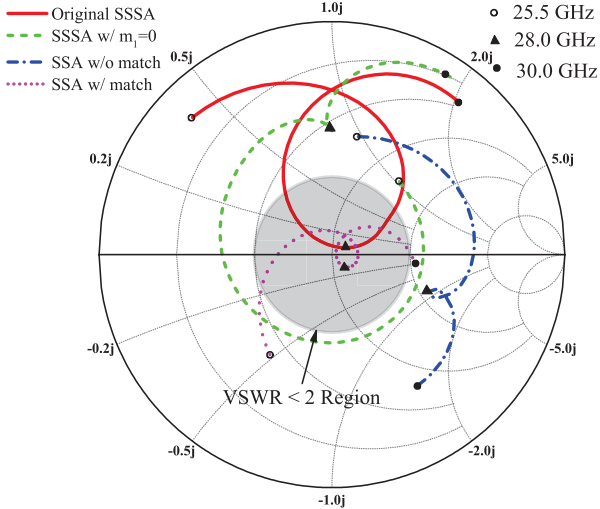
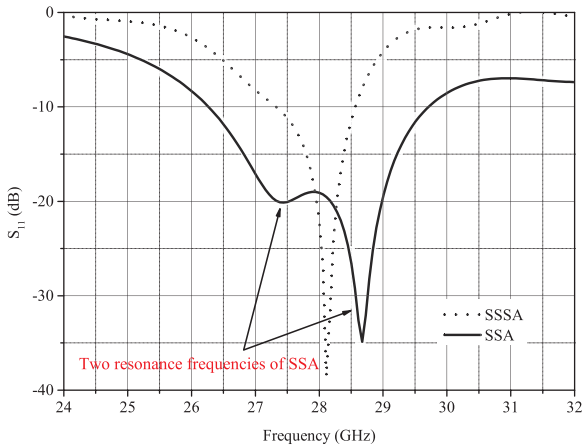


Fig. 6. Transformation of input impedance from the SSSA to the SSA.

Fig. 7. Simulated  $|S_{11}|$  of the proposed SSSA and SSA.

transformation of the input impedance from the original SSSA structure to the final SSA structure, where the  $w/$  denotes with, and the  $w/o$  represents without. The impedance locus of the SSSA with  $m_1 = 0$  and the SSA without the matching vias share the similar curve shape but a rotation in the Smith chart, which comes from the similar resonance characters of these two structures, and the modulating of the feeding via, as shown in Fig. 4. To improve the reflection coefficient of the SSA, the matching circuit is introduced in the antenna structure. This kind of impedance matching network formed by a row of metallic vias acts as a shunt inductor in a two-port network, which has already been clarified in [10] and [14].

Third, different from the SSSA, the SSA behaves as a much wider impedance bandwidth character. The simulated  $|S_{11}|$  of the SSSA and the SSA is shown in Fig. 7. The simulated impedance bandwidth ( $|S_{11}| \leq -10$  dB) of the SSA is  $\sim 12.1\%$ , which is wider than that of the SSSA. As shown in Fig. 6, two loops with similar shapes around the center frequency of 28 GHz are observed at the impedance locus of the SSSA with  $m_1 = 0$ , and the SSA without the matching circuit, respectively. It means that the broadband property of

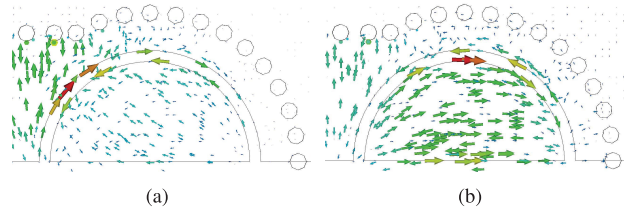
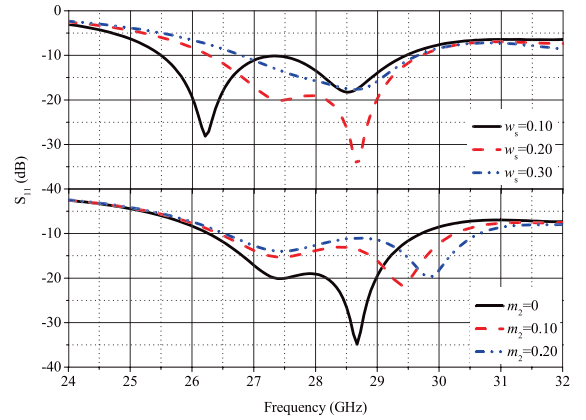


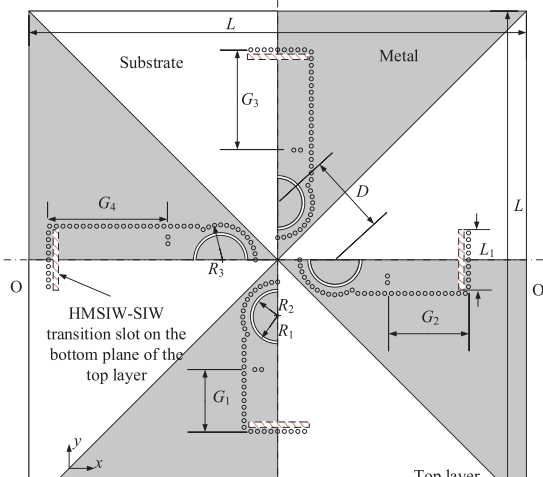
Fig. 8. Surface current distribution of the proposed SSA antenna at different frequencies. (a) 27.4 GHz. (b) 28.7 GHz.

Fig. 9. Reflection coefficient versus  $w_s$  when the inner radius of the slot  $r_5$  is fixed at 1.79 mm, and  $m_2$ .

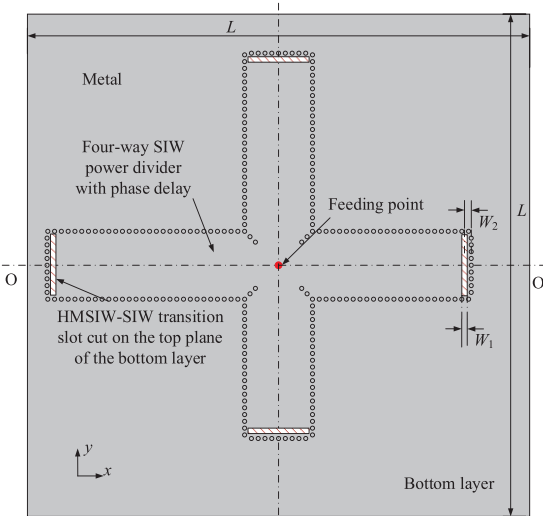
the input impedance of the SSA is inherent, but not due to the matching circuit. This broader  $|S_{11}|$  bandwidth performance comes from the dual-mode resonance of the SSA structure. By merging these two resonating modes close to each other, a wider impedance bandwidth is achieved.

As shown in Fig. 7, the antenna resonates at two frequencies: the lower frequency locates at around 27.4 GHz, while the higher one is about 28.7 GHz. The surface current distributions at these two frequencies are shown in Fig. 8. The resonances at these two frequencies can be explained intuitively by the two different combinations of the resonance of the semicircle slot (denoted by a slot mode) and the resonance of the semicircle patch inside the slot (denoted by a patch mode). At 27.4 GHz, hybrid mode I consists of a strong slot mode resonance and a weak patch mode resonance is excited, as shown in Fig. 8(a). At 28.7 GHz, the hybrid mode II consists of a strong slot mode resonance and a strong patch mode resonance is excited, as shown in Fig. 8(b).

The mode analysis is verified by the studies on the critical parameters  $w_s = r_4 - r_5$  and  $m_2$ . Fig. 9 shows the effects of  $w_s$  at the reflection coefficient of the SSA when the inner radius of the slot  $r_5$  is fixed, and the effects of  $m_2$  at the reflection coefficient when other parameters are fixed. When the inner radius of the slot  $r_5$  is fixed, the lower resonance frequency increases as  $w_s$  increases, which indicates that the lower resonance frequency is mainly affected by the dimensions of the semicircle slot. The higher resonance frequency decreases as  $m_2$  decreases, which indicates that the impedance bandwidth of the SSA will decrease when the dimension of the inner patch turns larger. This relationship between the patch size and the higher resonance frequency



(a)



(b)

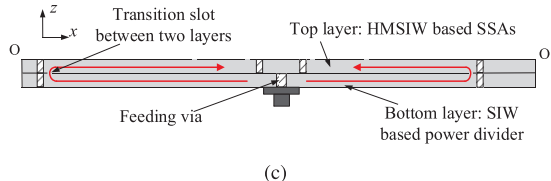


Fig. 10. Geometry of the proposed antenna array. (a) Top view of the top layer. (b) Bottom layer. (c) Cross-sectional view.

also explains the relatively narrower impedance bandwidth of the conventional SSSA, whose larger quasi-semicircle patch size leads to the combination of the two resonant frequencies. These two critical parameters of  $w_s$  and  $m_2$  can separately affect these two resonance frequency with a slight influence on the other, which offers a convenient way to modulate the reflection coefficient performance of the proposed SSA. As shown in Fig. 9, the broadest  $S_{11}$  bandwidth of about 14.5% can be achieved when  $w_s$  is set to 0.10. Considering the fabricated deviation and the AR performance, the  $w_s$  is set as 0.20.

TABLE III  
PARAMETERS OF THE PRESENTED SSA-BASED  $2 \times 2$  ANTENNA ARRAY

Parameter	Value (mm)	Parameter	Value (mm)
$L$	37.0	$L_1$	4.20
$D$	6.90	$W_1$	0.20
$G_1$	4.80	$W_2$	0.20
$G_2$	6.23	$R_1$	1.84
$G_3$	7.66	$R_2$	2.04
$G_4$	9.09	$R_3$	2.66

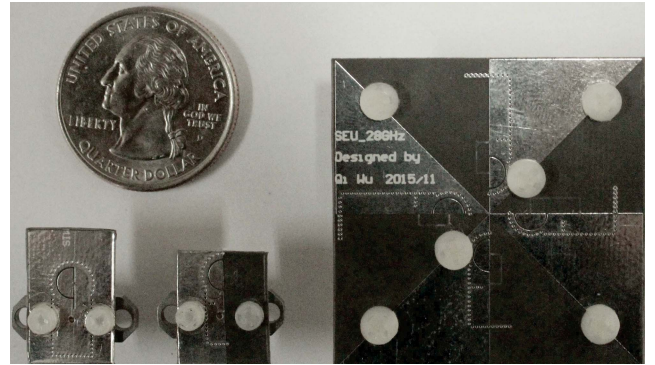


Fig. 11. Photograph of the fabricated SSSA, SSA, and SSA-based antenna array.

### III. PROTOTYPE VERIFICATION

In this section, the prototypes of the two antenna elements and a sequential rotated array based on the SSA element are designed and fabricated. In order to improve the bandwidth and enhance the CP gain, the SIW-based  $2 \times 2$  array antenna with sequential feeding scheme is fabricated using the geometry similar to [11], while applying a new SIW-HMSIW transition structure. The structure of the proposed sequential rotation antenna array is shown in Fig. 10. The parameters of the array are given in Table III. Four SSAs and  $90^\circ$  HMSIW phase-delay lines with a progressive phase shift are aligned in the top layer, as shown in Fig. 10(a). A four-way SIW power divider and phase-delay lines are aligned in the bottom layer, as shown in Fig. 10(b). The two-layer SIW-HMSIW transition is consist of two parallel waveguides sharing a common broad wall with a narrow transverse coupling slot, and is hereby used to avoid the physical connection between the different layers, and achieve better insertion loss performance at a wide frequency band.

The initial dimensions of the antenna elements and array are calculated using (1) and (2), which are then optimized using the CST microwave studio software [30]. The two antenna elements and the antenna array use single-layer Rogers Duroid 5880 substrate, whose thickness is  $h = 0.508$  mm, dielectric constant is  $\epsilon_r = 2.2$ , and loss tangent is 0.0009. The two layers of the antenna array are then fabricated using plastic studs. The photograph of the fabricated antenna elements and the antenna array is shown in Fig. 11.

### IV. RESULTS AND DISCUSSION

The simulated and measured results for the reflection coefficient, AR, and RHCP gain of the fabricated antennas are

TABLE IV  
MEASURED RADIATION PATTERN OF THE PROPOSED ANTENNAS

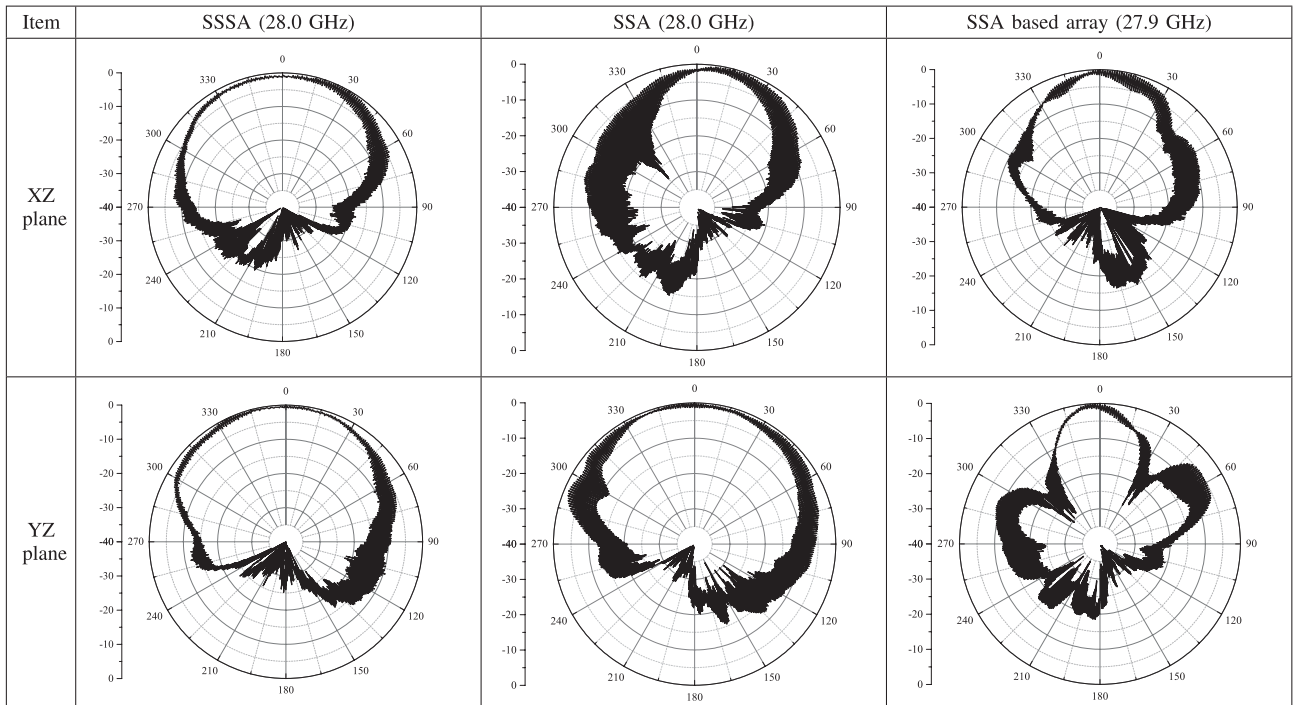


TABLE V  
PERFORMANCE COMPARISON OF THE CAVITY-BACKED SIW/HMSIW ANTENNAS AND ANTENNA ARRAYS

Item	Our work			Reference			
	SSSA	SSA	SSA based array	[12]	[14]	[16]	[11]
Technique	SIW	HMSIW	SIW based sequential rotation	SIW	SIW	HMSIW	SIW based sequential rotation
Frequency (GHz)	28.0	28.0	28.0	10.1	10.3	8.0	8.3
Size ( $\lambda_0$ )	$0.65 \times 0.51 \times 0.05$	$0.65 \times 0.26 \times 0.05$	$3.60 \times 3.60 \times 0.10$	$0.81 \times 0.81 \times 0.017$	$1.04 \times 1.04 \times 0.05$	$0.72 \times 0.36 \times 0.02$	$3.04 \times 3.04 \times 0.09$
Peak CP Gain (dBic)	5.9	5.3	10.8	6.3	7.8	4.2	10.9
-10 dB $ S_{11} $ Bandwidth	6.3%	12.1%	23.3%	3.0%	14.0%	6.0%	13.3%
3-dB AR Bandwidth	1.8%	2.3%	7.7%	0.8%	2.4%	0.7%	7.2%

shown in Fig. 12, which agree well. The AR is measured at the boresight direction of the proposed antennas. The measured results show that the reflection coefficient for the SSSA and the SSA are below  $-10$  dB for  $27.25\sim28.53$  GHz and  $25.72\sim29.25$  GHz, respectively. The measured minimum AR is 0.5 dB at 28 GHz for the SSSA, and is 1.2 dB at 28 GHz for the SSA. The measured fractional AR bandwidth for the SSSA and the SSA is 1.79% ( $27.85\sim28.25$  GHz) and 2.25% ( $27.69\sim28.32$  GHz), respectively. The measured gains of both antennas at their boresight directions are also shown in Fig. 12. The peak measured RHCP gain within the 3-dB AR bandwidth is nearly 5.85 and 5.26 dBic for the SSSA and the SSA, respectively. In addition, the fractional 3-dB gain bandwidth is 8% ( $26.65\sim28.80$  GHz) and 15% ( $25.55\sim29.70$  GHz), respectively. As for the SSA-based array, the measured reflection coefficient bandwidth is  $24.20\sim30.55$  GHz. The measured fractional AR bandwidth

is 7.7% ( $26.60\sim28.55$  GHz). The peak measured RHCP gain within the 3-dB AR bandwidth is  $\sim 10.77$  dBic at 27.9 GHz.

The measured spinning linear normalized radiation patterns of the proposed antennas in the  $xz$  plane and the  $yz$  plane are proposed in Table IV. It can be seen that the SSA presents similar radiation pattern with the SSSA in the  $yz$  plane, but with a narrower half power beamwidth radiation pattern in the  $xz$  plane. The measured front to back ratio of the SSSA and the SSA is about 25 and 20 dB, respectively.

A comparison between the measurement results of the proposed SSSA, SSA, and SSA-based antenna array with the previously reported antennas and antenna array based on the SIW-like backed cavities is presented in Table V, where  $\lambda_0$  refers to the free space wavelength at the operating frequency. The sizes of the antennas are measured by those of the SIW/HMSIW cavities, exclusive of the feeding structures, while considering the direction of them. As shown in Table V,

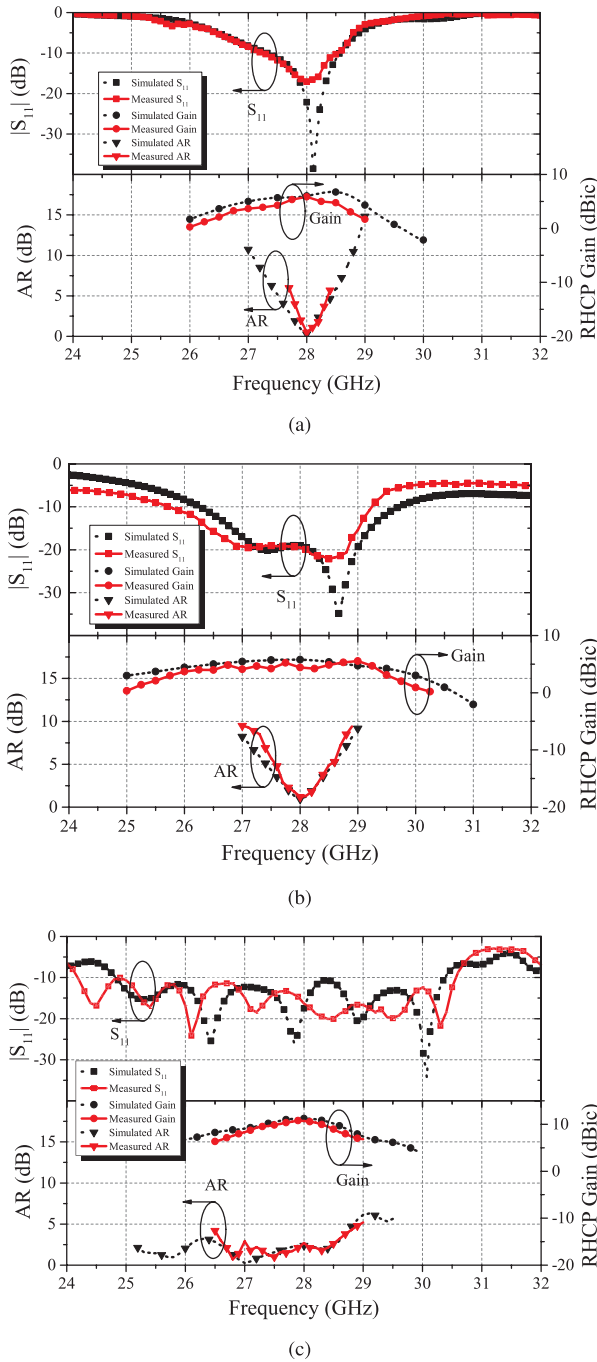


Fig. 12. Simulated and measured results of (a) SSSA, (b) SSA, and (c) array based on SSA.

with an easy design strategy without the matching circuit and a much smaller size, the SIW-based SSSA achieves a comparable gain and AR performance in a much higher frequency when compared with the previously reported SIW-cavity-based antennas. Moreover, with a further compact antenna size, the HMSIW-based SSA achieves a comparable antenna gain, AR bandwidth, and a broader reflection coefficient bandwidth with the conventional SIW-cavity-backed CP antenna. When compared with the previously reported HMSIW-cavity-backed antenna, the proposed SSA demonstrates the smaller size, higher CP gain, broader impedance, and AR bandwidth.

## V. CONCLUSION

Using the SIW-like structures, two new low-profile CP cavity-backed antennas and a sequential-rotated antenna array have been presented. A spoon-shaped slot structure has been used to excite CP radiation in the SIW cavity. Moreover, a novel SIW-HMSIW transformation method has been proposed to design the HMSIW-cavity-backed antenna based on the original SIW-cavity-backed antenna design. By making the edge of the HMSIW cavity equivalent to the longitudinal slot in the SIW cavity, a more compact HMSIW-cavity-backed antenna structure has been achieved. Two hybrid modes have been utilized and modulated to achieve broader impedance bandwidth. Next, using the novel two-layer HMSIW-SIW transitions, the SSA-based antenna array has been designed to validate the feasibility of the SSA for the array application. Design strategies for the SSSA and the SSA have also been proposed. It has been shown that the proposed SIW-based SSSA can achieve comparable radiation performance with a much compact size and simpler topology when compared with those of the previous SIW-cavity-backed designs. Finally, the simulation and measurement results show that the proposed HMSIW-cavity-backed SSA provides excellent features, including smaller size, higher gain, wider AR, and impedance bandwidth, when compared with the previously reported HMSIW-cavity based antenna, and can also be easily extended to array applications for wireless or satellite communication systems.

## ACKNOWLEDGMENT

The authors would like to thank the editor and the anonymous reviewers for their valuable comments and discussion. They would also like to thank their colleagues in the State Key Laboratory of Millimeter Waves, Southeast University, Nanjing, China, for their valuable discussions and support in measurement.

## REFERENCES

- [1] L. Wei, R. Q. Hu, Y. Qian, and G. Wu, "Key elements to enable millimeter wave communications for 5G wireless systems," *IEEE Wireless Commun.*, vol. 21, no. 6, pp. 136–143, Dec. 2014.
- [2] T. S. Rappaport *et al.*, "Millimeter wave mobile communications for 5G cellular: It will work!" *IEEE Access*, vol. 1, pp. 335–349, May 2013.
- [3] W. Hong, K.-H. Baek, Y. Lee, Y. Kim, and S.-T. Ko, "Study and prototyping of practically large-scale mmWave antenna systems for 5G cellular devices," *IEEE Commun. Mag.*, vol. 52, no. 9, pp. 63–69, Sep. 2014.
- [4] Q. Li, G. Wang, Z. Pan, and C.-L. I, "RF and antenna prototype for large scale antenna system," in *Proc. IEEE General Assembly Sci. Symp.*, Aug. 2014, pp. 1–4.
- [5] R. Ma, Y. Gao, L. Cuthbert, and Q. Zeng, "Antipodal linearly tapered slot antenna array for millimeter-wave base station in massive MIMO systems," in *Proc. IEEE Antennas Propag. Soc. Int. Symp.*, Jul. 2014, pp. 1121–1122.
- [6] Q. Li and Z. Shen, "An inverted microstrip-fed cavity-backed slot antenna for circular polarization," *IEEE Antennas Wireless Propag. Lett.*, vol. 1, no. 1, pp. 190–192, 2002.
- [7] H. Morishita, K. Hirasawa, and K. Fujimoto, "Analysis of a cavity-backed annular slot antenna with one point shorted," *IEEE Trans. Antennas Propag.*, vol. 39, no. 10, pp. 1472–1478, Oct. 1991.
- [8] D. Sievenpiper, H.-P. Hsu, and R. M. Riley, "Low-profile cavity-backed crossed-slot antenna with a single-probe feed designed for 2.34-GHz satellite radio applications," *IEEE Trans. Antennas Propag.*, vol. 52, no. 3, pp. 873–879, Mar. 2004.

- [9] W. Hong *et al.*, "SIW-like guided wave structures and applications," *IEICE Trans. Electron.*, vol. E92, no. 9, pp. 1111–1123, 2009.
- [10] D. Kim, J. W. Lee, C. S. Cho, and T. K. Lee, "X-band circular ring-slot antenna embedded in single-layered SIW for circular polarisation," *Electron. Lett.*, vol. 45, no. 13, pp. 668–669, Jun. 2009.
- [11] E.-Y. Jung, J. W. Lee, T. K. Lee, and W.-K. Lee, "SIW-based array antennas with sequential feeding for X-band satellite communication," *IEEE Trans. Antennas Propag.*, vol. 60, no. 8, pp. 3632–3639, Aug. 2012.
- [12] G. Q. Luo, Z. F. Hu, Y. Liang, L. Y. Yu, and L. L. Sun, "Development of low profile cavity backed crossed slot antennas for planar integration," *IEEE Trans. Antennas Propag.*, vol. 57, no. 10, pp. 2972–2979, Oct. 2009.
- [13] T. Zhang, W. Hong, Y. Zhang, and K. Wu, "Design and analysis of SIW cavity backed dual-band antennas with a dual-mode triangular-ring slot," *IEEE Trans. Antennas Propag.*, vol. 62, no. 10, pp. 5007–5016, Oct. 2014.
- [14] D.-Y. Kim, J. W. Lee, T. K. Lee, and C. S. Cho, "Design of SIW cavity-backed circular-polarized antennas using two different feeding transitions," *IEEE Trans. Antennas Propag.*, vol. 59, no. 4, pp. 1398–1403, Apr. 2011.
- [15] Q. Lai, C. Fumeaux, W. Hong, and R. Vahldieck, "Characterization of the propagation properties of the half-mode substrate integrated waveguide," *IEEE Trans. Microw. Theory Techn.*, vol. 57, no. 8, pp. 1996–2004, Aug. 2009.
- [16] S. A. Razavi and M. H. Neshati, "Development of a low-profile circularly polarized cavity-backed antenna using HMSIW technique," *IEEE Trans. Antennas Propag.*, vol. 61, no. 3, pp. 1041–1047, Mar. 2013.
- [17] N. Nguyen-Trong, T. Kaufmann, and C. Fumeaux, "A wideband omnidirectional horizontally polarized traveling-wave antenna based on half-mode substrate integrated waveguide," *IEEE Antennas Wireless Propag. Lett.*, vol. 12, pp. 682–685, 2013.
- [18] Y. Dong and T. Itoh, "Composite right/left-handed substrate integrated waveguide and half mode substrate integrated waveguide leaky-wave structures," *IEEE Trans. Antennas Propag.*, vol. 59, no. 3, pp. 767–775, Mar. 2011.
- [19] J. Xu, W. Hong, H. Tang, Z. Kuai, and K. Wu, "Half-mode substrate integrated waveguide (HMSIW) leaky-wave antenna for millimeter-wave applications," *IEEE Antennas Wireless Propag. Lett.*, vol. 7, pp. 85–88, 2008.
- [20] S. Agneessens and H. Rogier, "Compact half diamond dual-band textile HMSIW on-body antenna," *IEEE Trans. Antennas Propag.*, vol. 62, no. 5, pp. 2374–2381, May 2014.
- [21] J.-Y. Sze, C.-I. G. Hsu, and S.-C. Hsu, "Design of a compact dual-band annular-ring slot antenna," *IEEE Antennas Wireless Propag. Lett.*, vol. 6, pp. 423–426, 2007.
- [22] R. Li, B. Pan, A. N. Traillle, J. Papapolymerou, J. Laskar, and M. M. Tentzeris, "Development of a cavity-backed broadband circularly polarized slot/strip loop antenna with a simple feeding structure," *IEEE Trans. Antennas Propag.*, vol. 56, no. 2, pp. 312–318, Feb. 2008.
- [23] M.-H. Yeh, P. Hsu, and J.-F. Kiang, "Analysis of a CPW-fed slot ring antenna," in *Proc. Asia-Pacific Microw. Conf. (APMC)*, vol. 3, pp. 1267–1270, 2001.
- [24] W.-S. Chen, C.-C. Huang, and K.-L. Wong, "Microstrip-line-fed printed shorted ring-slot antennas for circular polarization," *Microw. Opt. Technol. Lett.*, vol. 31, no. 2, pp. 137–140, 2001.
- [25] K. F. Lee and W. Chen, *Advances in Microstrip and Printed Antennas*. New York, NY, USA: Wiley, 1997.
- [26] P. S. Hall, "Application of sequential feeding to wide bandwidth, circularly polarised microstrip patch arrays," *IEE Proc. H-Microw., Antennas Propag.*, vol. 136, no. 5, pp. 390–398, Oct. 1989.
- [27] S.-L. S. Yang, R. Chair, A. A. Kishk, K.-F. Lee, and K.-M. Luk, "Study on sequential feeding networks for subarrays of circularly polarized elliptical dielectric resonator antenna," *IEEE Trans. Antennas Propag.*, vol. 55, no. 2, pp. 321–333, Feb. 2007.
- [28] D. M. Pozar, *Microwave Engineering*. New York, NY, USA: Wiley, 2009.
- [29] J. Heikkinen and M. Kivikoski, "Low-profile circularly polarized rectifying antenna for wireless power transmission at 5.8 GHz," *IEEE Microw. Wireless Compon. Lett.*, vol. 14, no. 4, pp. 162–164, Apr. 2004.
- [30] *Computer Simulation Technology*, CST Microwave Studio, Framingham, MA, USA, 2009.



**Qi Wu** (S'15) was born in 1993. He received the B.S. degree in communication engineering from the Communication University of China, Beijing, China, in 2012, and the M.S. degree in electrical engineering from Southeast University, Nanjing, China, in 2015, where he is currently pursuing the Ph.D. degree in electrical engineering.

His current research interests include microwave and millimeter-wave passive components and antennas for future wireless mobile communications.



**Haiming Wang** (M'08) was born in 1975. He received the M.S. and Ph.D. degrees in electrical engineering from Southeast University, Nanjing, China, in 2002 and 2009, respectively.

He joined the State Key Laboratory of Millimeter Waves, Southeast University, in 2002, where he is currently an Associate Professor. In 2008, he was a short-term Visiting Scholar with the Blekinge Institute of Technology, Karlskrona, Sweden. His current research interests include radio propagation measurement and channel modeling, signal processing and multiple-input multiple-output wireless communications, and millimeter-wave wireless communications.

Dr. Wang received the first-class Science and Technology Progress Award of Jiangsu Province of China in 2009. He serves as the Vice Chair of the IEEE 802.11aj Task Group.



**Chen Yu** (M'11) was born in 1979. She received the M.S. and Ph.D. degrees in electrical engineering from Southeast University, Nanjing, China, in 2004 and 2011, respectively.

She joined the State Key Laboratory of Millimeter Waves, Southeast University, in 2004, where she is currently an Associate Professor. In 2007, she was a short-term Visiting Scholar with the Kalmar Institute of Technology, Kalmar, Sweden. Her current research interests include antennas and antenna arrays for wireless mobile communications

and radars.

Dr. Yu received the first-class Science and Technology Progress Award of Jiangsu Province of China in 2009.



Wei Hong (M'92–SM'07–F'12) received the B.S. degree from the University of Information Engineering, Zhengzhou, China, in 1982, and the M.S. and Ph.D. degrees from Southeast University, Nanjing, China, in 1985 and 1988, respectively, all in radio engineering.

He has been with the State Key Laboratory of Millimeter Waves, Southeast University, since 1988, where he has also been the Director of the Laboratory since 2003. He is currently a Professor and the Dean of the School of Information Science and Engineering with Southeast University. In 1993, 1995, 1996, 1997, and 1998, he was a short-term Visiting Scholar with the University of California at Berkeley, Berkeley, CA, USA, and the University of California at Santa Cruz, Santa Cruz, CA, USA. He has authored or co-authored over 200 technical publications and authored two books. His current research interests include numerical methods for electromagnetic problems, millimeter-wave theory and technology, antennas, electromagnetic scattering, and RF technology for mobile communications.

Dr. Hong was a three-time recipient of the first-class Science and Technology Progress Prizes by the Ministry of Education of China and the Jiangsu Province Government, China. He also received the Foundations for China Distinguished Young Investigators and for Innovation Group by the NSF of China. He serves as the Vice President of the Microwave Society and Antenna Society of the CIE, the Chair of the IEEE MTT/AP/EMC Joint Nanjing Chapter, and the AdCom Member of the IEEE Microwave Theory and Techniques Society, and served as the Associate Editor of the IEEE TRANSACTIONS ON MICROWAVE THEORY AND TECHNIQUES from 2007 to 2010.